coatings

Article

Comparative Study on Thermal Transmission Aspects of Nano and Ferrofluid in Enclosures Holding Heat-Generating Body

Umadevi Periyasamy [1], Nazek Alessa [2], G. Sadhana [1] and Karuppusamy Loganathan [3,*]

[1] Department of Mathematics, Dr. N. G. P. Arts and Science College, Coimbatore 641048, Tamilnadu, India
[2] Department of Mathematical Sciences, College of Sciences, Princess Nourah Bint Abdulrahman University, P.O. Box 84428, Riyadh 11671, Saudi Arabia
[3] Department of Mathematics and Statistics, Manipal University Jaipur, Jaipur 303007, Rajasthan, India
* Correspondence: loganathankaruppusamy304@gmail.com

Abstract: The heat-transmission characteristics of Co ferrofluid and $SiO_2 - water$ nanofluid are compared numerically inside enclosures including a heat-generating body. Using the finite-volume method, a steady laminar incompressible flow in two dimensions is solved. The numerical study is conducted to determine the impacts of the solid volume fraction ($\varphi = 0.02, 0.1$ and 0.2), the temperature-difference ratio ($\Delta T^* = 0, 4$ and 20), and the Rayleigh number ($Ra = 10^5, 10^6$ and 10^7) on both $SiO_2 - water$ nanofluid and Co ferrofluid, respectively. In consideration of isothermal and streamlines contours, the aspects of temperature transmission and fluid flow are addressed. It is shown that there is no remarkable difference in the convection rate for both the fluids while increasing the Rayleigh number and temperature difference ratio.

Keywords: ferro particle; heat-generating body; nanofluid; Rayleigh number; sinusoidal heating; temperature-difference ratio

check for updates

Citation: Periyasamy, U.; Alessa, N.; Sadhana, G.; Loganathan, K. Comparative Study on Thermal Transmission Aspects of Nano and Ferrofluid in Enclosures Holding Heat-Generating Body. *Coatings* **2022**, *12*, 1810. https://doi.org/10.3390/coatings12121810

Academic Editor: Ludmila B. Boinovich

Received: 28 September 2022
Accepted: 18 November 2022
Published: 24 November 2022

1. Introduction

Heat-transmission characteristics along a heat-generating source in enclosures have received growing attraction due to their engineering applications. Convection happens as a result of numerous man-made and natural factors: air conditioning, stream turbines, central heating, heat exchangers, car radiators, aerodynamic heating, convection ovens, blood circulation, shock, and waves. The transfer of heat energy is a crucial step in a wide range of industrial operations. Heat must be added, withdrawn, or transferred from one process stream to another throughout any industrial plant. This is now a crucial industrial necessity. These procedures offer a source for process fluid heating or cooling as well as energy recovery. The improvement of heating or cooling in an industrial process may result in energy savings, shorter processing times, higher thermal ratings, and longer equipment life. The viscosity of concentrated liquids and suspensions has received significant attention recently. The focus is now on suspended particles and their thermo-physical characteristics. The transfer of heat energy is a crucial step in a wide range of industrial operations. Heat must be added, withdrawn, or transferred from one process stream to another throughout any industrial plant. This is now an industrial necessity. These procedures offer a source for process fluid heating or cooling as well as energy recovery. One of the initiative works comparing the convection phenomenon of various suspensions will be the current paper.

Jahanshahi et al. [1] investigated heat-distribution intensification in enclosure subject to various heatings of side wall filled with SiO_2 nanofluid. They found that the unpredictable nature of various formulas that incorporate the nanofluid's effective thermal conductivity has an enormous influence on the enclosure's natural convective heat-transportation properties. The convective flow and heat distribution in enclosures along fractionally dynamic horizontal walls replete with Cu nanofluid was probed numerically by Sheikhzadeh et al. [2]. They came to the conclusion that the thermal distribution frequency deepens as the size factor of the nanoparticle rises for all tested Rayleigh numbers, with the dynamic top–bottom partitions of the horizontal walls experiencing the least average Nusselt number. Convective thermal transmission in a 2D enclosure utilizing CuO nanofluid was simulated numerically by Aminossadati and Ghasemi [3]. Their observation revealed that as the size factor of the nanofluid increases, heat distribution frequency likewise increases, strengthening Rayleigh number results in heavier streamlines inside the enclosure.

The characteristics of convection in nanofluids were reviewed by Haddad et al. [4]. They noticed that a lot of the numerical findings demonstrate that nanofluids automatically boost the efficiency of conventional heat distribution in fluid. However, the findings of the experiments indicated that the presence of nanoparticles consistently disrupts heat transportation. The natural convection of nanofluids with hot and cold side walls, or with the bottom wall heating uniformly or unevenly and the cold side walls occupying the heat flow visualization via heat functions or heat lines, was investigated by Basak and Chamkha [5]. Their findings showed that for all the Ra values, the convective heat transmission was eminently strong for nanofluids and the Nusselt number for nanofluids exhibits greater scores correlated to those of water. Garoosi et al. [6] studied the nanofluids, which were combined with convection in a square enclosure that has both internal and external heating modeled as a two-phase mixture. They discovered that thermal distribution frequency spontaneously diverges when HAC is placed in an immobile position and that the size factor of nanoparticles maximizes thermal transmission.

Hasan et al. [7] observed a mixed convection heat distribution surrounded by an enclosure along the $Cu - water$ nanofluid. They found that a higher heat distribution was attained during the convection effect, corresponding to a buoyancy number exceeding 10^3. Umadevi and Nithyadevi [8] investigated the convection using a heat-generating body and $Ag - water$ nanofluid in a sinusoidally hot enclosure. They found that the Nusselt number graph increases with increasing ΔT^*. A study of convective thermal distribution for two different nanofluids with a partly heated regular-cylindrical-shaped enclosure was numerically conducted by Guestal et al. [9]. They reported that the outflow concentration and the thermal transmission increase as the Ra increases and that as the heater length lengthens, the heat transfer rises. The thermal performance of a nanofluidic $Cu - water$ -free convective electronic dome enclosed in a tilted hemispherical enclosure was examined by Bairi et al. [10]. Their results showed that certain combos of Rayleigh number, tilting angle, and size factor were unworkable in a stable operating environment for a regular system necessitating thermo-regulation. The advanced-temperature Rayleigh–Prandtl-angle-type correlation simplifies electrical assembly's thermal design under consideration. Mashayekhi et al. [11] carried out CFD research on hybrid vehicles' thermal and hydrodynamic properties in a sinusoidal double-layered microchannel heat sink with nanofluid as the fluid. They conformed that shear stress is raised by increasing fluid viscosity, particularly in places near walls and in fluid layers. They also showed that components can increase the pressure drop in larger solid nanoparticle volume fractions and in lower Reynolds numbers and in hot surfaces, and that their sinusoidal forms have an impact on the static temperature profiles. Under local thermal non-equilibrium conditions, the heat and fluid flow analysis of metal foam embedded in a double-layered sinusoidal heat sink was performed by Arasteh et al. [12]. Investigation into the reliability of the local thermal equilibrium (LTE) hypothesis revealed that, under LTE conditions, increasing the Darcy number, which increases porous particle width, negatively affects the results.

Al-Srayyih et al. [13] numerically analyzed the impact of the left wall that was vertically heated on convection discharge in enclosure filled with nanofluid penetrable layers using the Galerkin finite-element method. Researchers noticed that low heat conductance proportion values imply greater heat-transfer intensification than higher thermal conductivity ratio values. Latifa et al. [14] did a study the distribution of convection heat in an enclosure along magnetic nanoparticles and noted that the thermal Rayleigh number's higher values influence the average Nusselt number, the nanoparticle shape factor, and the nanoparticle volume percentage. The generalized-finite-difference-method-based numerical results on equations of coupled unstable nonlinear convection and diffusion were examined by Fu et al. [15]. They came to the conclusion that the proposed generalized finite difference method might be considered as a simple and competitive option for solving these convection-diffusion equations. Massoudi [16] investigated whether MHD convective heat transfer and radiation occur inside an inclined, diamond-water filled trapezoidal enclosure and a spinning elevated baffle. Through their obtained data, they suggested that the increasing Rayleigh number value, the baffle radius, and the radiation enhance the convection frequency of heat.

Increasing the Hartmann number lowers the frequency of heat. The existence of homogeneous thermal generation improves the cavity's thermal transmission and promotes buoyancy, while the consistent heat uptake lowers it and utilizing nanoparticles of a larger shape factor enhances the convective thermal transmission more. According to Lee and Kim's [17] analysis of the flow characteristics inside the ferrofluid-filled rectangular enclosure along the impact of irregular magnetic fields, a vortex was formed in the places with a strong magnetic field intensity. Mourand et al. [18] numerically examined the naturally occurring convection of nanofluid from elliptical cylinders in a wavy enclosure whenever a magnetic field was constantly active. Their findings exposed that increasing the Rayleigh number, Darcy number, or solid-volume fraction enhances thermal transmission. While the Hartmann number was changed from 0 to 100, the Nusselt number's values were reduced by up to 22.22 percent, and a 45-degree inclination angle was ideal for the convection process. Chandanam et al. [19] carried out the numerical investigation on thermal control in a triangular porous cavity that had hot obstacles filled with air under convective heat transfer. They observed that isotherms were normally parallel to the inclined wall at lower Rayleigh numbers and were altered significantly at the obstructions at the vertical left insulated wall. Nevertheless, as the Rayleigh number increased, those deformations became more noticeable in the core, relatively warm zones scattered towards the inclined cold wall, and the simulations were useful in the processing of magnetic materials and the development of hybrid magnetic fuel cells. MHD's impact on the rate of heat transfer through ferrofluid in a square cavity with a heat source or obstacle was studied by Javed and Siddiqui [20]. They concluded that Ra increase causes the strength of the streamline to increase. Circulations as isotherms demonstrate convection by being a severely distorted dominating phase for large Rayleigh numbers in the cavity. Heated ferrofluid has a higher rate than normal fluid and its aspect increases. Additionally, the magnitude of stream-line circulations is decreased by the ratio of square blockage. Some recent references are seen in [21–25]

This article compares the effects of heat transfer between a $SiO_2 - water$ nanofluid and Co ferrofluid inside an enclosure that involves a body that generates heat and has a variety of thermal boundaries. The top wall is insulated; the heated left wall is sinusoidally heated; the right wall is cold; and the bottom wall is uniformly heated. The velocity and behavior of heat flux are studied using isotherms and streamlines. There have been many studies published on the convection heat transfer in enclosures with nanofluid and ferrofluids along barriers. No study has compared the effects of using various fluids along heat-generating obstructions. Moreover, future work can be extended with the magnetic field effect, entropy generation, and the inclination of the enclosure.

2. Problem Definition

2.1. Configuration

For the present study, it is supposed that the flow is steady, laminar, and has constant fluid properties in two dimensions, and Figure 1 shows the boundary conditions and the problem's schematic. This structure comprises a solid L-length square enclosure, a body with width W, and thermal conductivity k_s that generates heat. The enclosure's left wall has sinusoidal heating as $T'_{sin} = T'_c + (T'_h - T'_c) A \sin^2\left(\frac{2\pi y'}{L}\right)$ and an insulated top horizontal wall. The right wall is applied at a uniform cool temperature T'_c, while a constant heated temperature T_h' is maintained on the bottom wall, and at every circumstance, the condition $T_h' > T_c'$ is maintained. The model formulated is used to present the comparitive study of the effect of the heat distribution of $SiO_2 - water$ nanofluid and Co ferrofluid. Since there is supposed to be thermal equilibrium between water and nanoparticles, it is claimed that all rigid boundaries are no slip walls. Nanoparticles' (SiO_2 and Co) and the base fluid's thermophysical characteristics are shown in Table 1. Radiation effects are disregarded since gravity interacts with matter in a downward y direction.

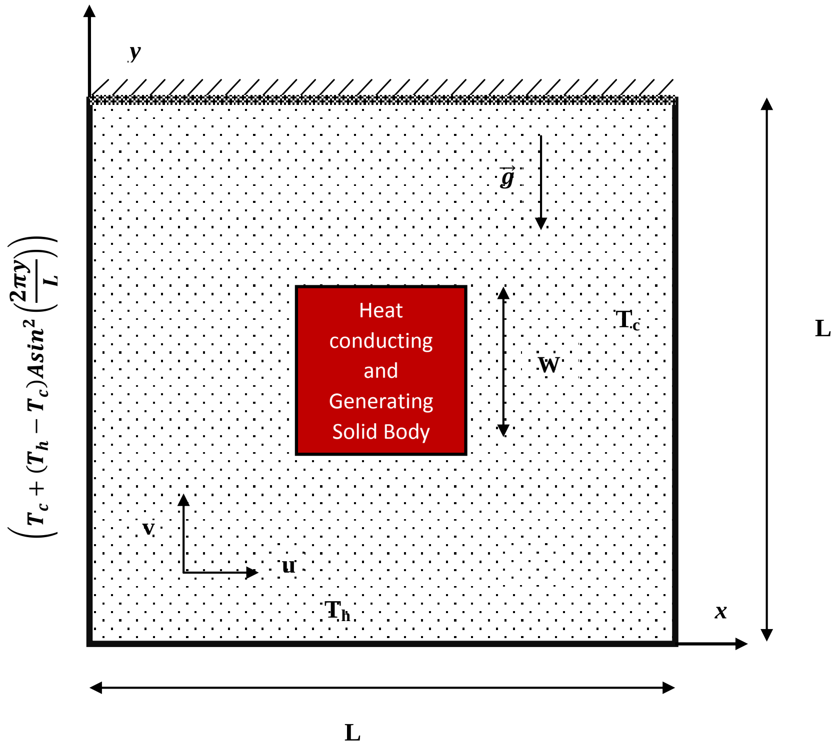

Figure 1. Schematic representation of the computational domain.

Table 1. Thermo physical properties of water and nanoparticles at room temperature.

	ρ (kg/m^3)	C_p (J/kg·K)	k (W/m·K)	$\beta \times 10^5$ (K^{-1})
Pure water	997.1	4179	0.613	21
Sio_2	3970	765	36	0.63
Co	8900	420	100	1.3

2.2. Governing Equations

The analytical expressions of Javed and Siddiqui [20] are approximated by the Boussinesq method for the flow of fluid, and the thermal distribution of nanofluid can also be interpreted as

The continuity equation

$$\frac{\partial u'}{\partial x'} + \frac{\partial v'}{\partial y'} = 0 \tag{1}$$

The momentum equations are

$$\rho_{nf}\left(u'\frac{\partial u'}{\partial x'} + v'\frac{\partial u'}{\partial y'}\right) = -\frac{\partial p'}{\partial x'} + \mu_{nf}\left(\frac{\partial^2 u'}{\partial x'^2} + \frac{\partial^2 u'}{\partial y'^2}\right) \tag{2}$$

$$\rho_{nf}\left(u'\frac{\partial v'}{\partial x'} + v'\frac{\partial v'}{\partial y'}\right) = -\frac{\partial p'}{\partial y'} + \mu_{nf}\left(\frac{\partial^2 v'}{\partial x'^2} + \frac{\partial^2 v'}{\partial y'^2}\right) + g(\rho\beta)_{nf}(T' - T_c') \tag{3}$$

The energy equation

$$u'\frac{\partial T'}{\partial x'} + v'\frac{\partial T'}{\partial y'} = \alpha_{nf}\left(\frac{\partial^2 T'}{\partial x'^2} + \frac{\partial^2 T'}{\partial y'^2}\right) \quad (4)$$

The energy equation for the heat-conducting body [26]

$$k_s\frac{\partial^2 T'_s}{\partial x'^2} + k_s\frac{\partial^2 T'_s}{\partial y'^2} + \dot{q} = 0 \quad (5)$$

where,

The nanofluid's density can always be determined via

$$\rho_{nf} = \rho_s\varphi + \rho_f(1-\varphi) \quad (6)$$

and φ indicates the solid size factor of the nanoparticle

The heat capacity of nanofluid can be calculated by

$$(\rho C_p)_{nf} = (\rho C_p)_s\varphi + (\rho C_p)_f(1-\varphi), \quad (7)$$

The nanofluid's heat expansion coefficient can be calculated using

$$(\rho\beta)_{nf} = (\rho\beta)_s\varphi + (\rho\beta)_f(1-\varphi), \quad (8)$$

$$\alpha_{nf} = \frac{k_{nf}}{(\rho C_p)_{nf}}, \quad (9)$$

$$\beta_{nf} = \beta_s\varphi + \beta_f(1-\varphi), \quad (10)$$

The determination of the nanofluid's viscosity via Brinkman's Formula [27]

$$\mu_{nf} = \frac{\mu_f}{(1-\varphi)^{2.5}}, \quad (11)$$

The evaluation of the nanofluid's heat conduct efficiency via Maxwell's formula [28]

$$\frac{k_{nf}}{k_f} = \left[\frac{(k_s + 2k_f) - 2\varphi(k_f - k_s)}{(k_s + 2k_f) + \varphi(k_f - k_s)}\right] \quad (12)$$

The dimensional form of dynamic and thermal boundaries are

$$\begin{aligned}
x' &= 0,\quad 0 \le y' \le L: \quad u' = v' = 0,\quad T' = T'_{sin} = T'_c + (T'_h - T'_c)A sin^2\left(\frac{2\pi y'}{L}\right)\\
x' &= L,\quad 0 \le y' \le L: \quad u' = v' = 0,\quad T' = T'_c\\
y' &= 0,\quad 0 \le x' \le L: \quad u' = v' = 0,\quad T' = T'_h\\
y' &= L,\quad 0 \le x' \le L: \quad u' = v' = 0,\quad \frac{\partial T'}{\partial y'} = 0
\end{aligned}$$

At the fluid–solid interface's boundaries:

$$k_{nf}\left(\frac{\partial T'}{\partial n}\right)_{nanofluid} = k_s\left(\frac{\partial T'}{\partial n}\right)_{solid} \quad (13)$$

Variables and parameters without dimensions are:

$$(X', Y') = \frac{(x', y')}{L}; \quad P' = \frac{(p' + \rho_0 g y')L^2}{\rho_{nf}\alpha_f^2}; \quad (U', V') = \frac{(u', v')L}{\alpha_f}; \quad \theta' = \frac{T' - T'_c}{T'_h - T'_c}$$

The Prandtl number $(Pr) = \frac{\nu_f}{\alpha_f}$ (the ratio of momentum diffusivity to thermal diffusivity); the Rayleigh Number $Ra = \frac{g\beta_f(T'_h - T'_c)L^3}{\nu_f \alpha_f}$ (associated with buoyancy-driven flow; it can be expressed as the product of the Grashof number and the Prandtl number); the area ratio $A^* = \frac{W^2}{L^2}$ (the ratio between the square of the width of the solid body to the square of the length of an enclosure); $K^* = \dfrac{k_s}{k_{nf}}$(the thermal conductivity ratio between the solid and the fluid); and the temperature-difference ratio of the solid and the fluid $\Delta T^* = \frac{(\frac{\dot{q}W^2}{K_{nf}})}{T'_h - T'_c}$.

The mathematical model used to build the pertinent dimensionless forms is as follows:

$$\frac{\partial U'}{\partial X'} + \frac{\partial V'}{\partial Y'} = 0 \tag{14}$$

$$U'\frac{\partial U'}{\partial X'} + V'\frac{\partial U'}{\partial Y'} = -\frac{\partial P'}{\partial X'} + \frac{\mu_{nf}}{\rho_{nf}\alpha_f}\left(\frac{\partial^2 U'}{\partial X'^2} + \frac{\partial^2 U'}{\partial Y'^2}\right) \tag{15}$$

$$U'\frac{\partial V'}{\partial X'} + V'\frac{\partial V'}{\partial Y'} = -\frac{\partial P'}{\partial Y'} + \frac{\mu_{nf}}{\rho_{nf}\alpha_f}\left(\frac{\partial^2 V'}{\partial X'^2} + \frac{\partial^2 V'}{\partial Y'^2}\right) + \frac{(\rho\beta)_{nf}}{\rho_{nf}\beta_f} PrRa\theta' \tag{16}$$

$$U'\frac{\partial \theta'}{\partial X'} + V'\frac{\partial \theta'}{\partial Y'} = \frac{\alpha_{nf}}{\alpha_f}\left(\frac{\partial^2 \theta'}{\partial X'^2} + \frac{\partial^2 \theta'}{\partial Y'^2}\right) \tag{17}$$

The equation of energy for a solid heat-generating body

$$K^*\left(\frac{\partial^2 \theta'_s}{\partial X'^2} + \frac{\partial^2 \theta'_s}{\partial Y'^2}\right) + \frac{\Delta T^*}{A^*} = 0 \tag{18}$$

Accordingly, the following are the dimensionless boundary conditions

$$\begin{aligned}
X' &= 0, \quad 0 \le Y' \le 1: \quad U' = V' = 0, \quad \theta' = A\sin^2(2\pi Y') \\
X' &= 1, \quad 0 \le Y' \le 1: \quad U' = V' = 0, \quad \theta' = 0 \\
Y' &= 0, \quad 0 \le X' \le 1: \quad U' = V' = 0, \quad \theta' = 1 \\
Y' &= 1, \quad 0 \le X' \le 1: \quad U' = V' = 0, \quad \frac{\partial \theta'}{\partial Y'} = 0
\end{aligned}$$

Dimensionless bounding circumstance at the interface between solid and fluid:

$$\left(\frac{\partial \theta'}{\partial N}\right)_{nanofluid} = K^*\left(\frac{\partial \theta'}{\partial N}\right)_{solid} \tag{19}$$

The ratio of conductive to convective heat transfer at a fluid boundary is known as the Nusselt number. Advection (fluid movement) and diffusion are both a part of convection (conduction). For a presumably immobile fluid, the conductive element is measured under the same circumstances as the convective component. It is a dimensionless number that is connected to the Rayleigh number of the fluid.

$$\overline{Nu}_{leftwall} = \overline{Nu}_{rightwall} = \int_0^1 \left(-\frac{k_{nf}}{k_f}\frac{\partial \theta'}{\partial X'}\right)_{wall} dY'.$$

$$\overline{Nu}_{bottomwall} = \int_0^1 \left(-\frac{k_{nf}}{k_f}\frac{\partial \theta'}{\partial Y'}\right)_{Y'=0} dX'.$$

3. Method of Solution

The finite-volume method has been used to solve the governing nonlinear equations along the iterative numerical method with the necessary boundary conditions. Patankar's [29]

SIMPLE algorithm (Semi-Implicit Method for Pressure-Linked Equations) is employed to couple pressure and velocity which is a technique for solving the Navier–Stokes equations numerically. Diffusion and convection terms were transmitted using the power-law strategy. The set of discretized equations has been iteratively solved using the tri-diagonal matrix algorithm (TDMA), and the under-relaxation approach has been employed to ensure easy convergence. Every control volume's mass residue has also been measured, and the optimum value is frequently used to assess convergence. The solution process is carried out until the following convergence condition is satisfied: $\frac{\lambda_{i,j}^{n+1}-\lambda_{i,j}^{n}}{\lambda_{i,j}^{n+1}} < 10^{-6}$, where u', v', and T' are indicated by the standard variable λ.

4. Validation Study

Numerical research is carried out using the established finite-volume-method-dependent FORTRAN 77 coding. The conventional coding was thoroughly verified using nanofluids inside the enclosure with Cheikh's et al. [30] non-uniform bottom wall heating approach for $A_2O_3 - water$ nanofluid along with distinct φ and Ra. Table 2 compares the value of the Nusselt number. The outcomes from previous presentations were found to be in better agreement with the current numerical results. To determine the influence of the numerical efficiency on the grid sizes, a self-reliance test was carried out, and a staggered grid arrangement with six odd grid sizes from 91×91 to 141×141 was chosen for the current assessment. Grids 131×131 and 141×141 reflect the closer outcome, and grid 131×131 was chosen for the final calculation. The grid independent test is shown in Figure 2.

Table 2. Nusselt number at hot wall for Al_2O_3 with various Ra and φ Cheik et al. [30].

Ra	$\varphi = 0.05$		$\varphi = 0.1$		$\varphi = 0.15$		$\varphi = 0.20$	
	Cheik et al. [30]	**Present**	**Cheik et al. [30]**	**Present**	**Cheik et al. [30]**	**Present**	**Cheik et al. [30]**	**Present**
5×10^3	2.522	2.520	2.809	2.811	3.161	3.160	3.575	3.571
5×10^4	5.148	5.145	5.400	5.403	5.607	5.609	5.762	5.760
5×10^5	9.158	9.157	9.680	9.683	10.18	10.182	10.66	10.661

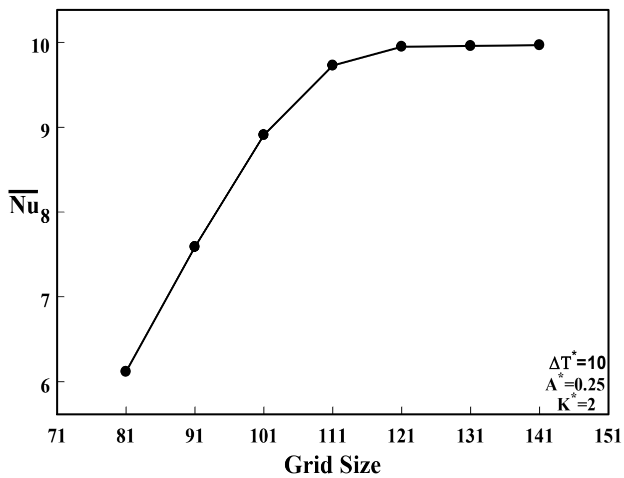

Figure 2. Grid independence test.

5. Results and Discussion

Effect of heat transfer between $SiO_2 - water$ nanofluid and a Co ferrofluid inside square enclosure along a heat-generating body is compared in this paper for various Rayleigh numbers ($Ra = 10^4, 10^5$ and 10^6), the solid volume fraction ($\varphi = 0.02, 0.1$ and 0.2), and the temperature-difference ratio ($\Delta T^* = 0, 4$ and 20). Here, the area ratio $A^* = 0.25$ and the thermal conductivity ratio $K^* = 2$ are kept fixed.

Figure 3 illustrates the comparison between the the streamlines of $SiO_2 - water$ nanofluid and Co ferrofluid for $10^4 \leq Ra \leq 10^6$ and $\Delta T^* = 0, 4$ and 20 with the fixed solid volume fraction ($\varphi = 0.02$) where the dotted lines represent the $SiO_2 - water$ nanofluid and the solid lines represents the Co ferrofluid. When comparing the streamlines of different Rayleigh numbers, most of the dotted and solid lines coincide with each other. For the cases $\Delta T^* = 0, Ra = 10^4$ and $\Delta T^* = 0, Ra = 10^5$, since the buoyancy force is incapacitated, the streamlines constrict and are restricted to the enclosure's walls. For the cases $\Delta T^* = 0, Ra = 10^6$ and $\Delta T^* = 4, Ra = 10^4$, the streamlines are located on the left of the body that produces heat due to the increase in the temperature-difference ratio. When $\Delta T^* = 4$ and $Ra = 10^5$, adjacent to the right cold and the left sinusoidal wall, a tiny eddy develops that initiates motion in the fluid while the Rayleigh number is boosted. For the cases $\Delta T^* = 4, Ra = 10^5$, and $\Delta T^* = 20, Ra = 10^4$, a significant variation appears in the streamline pattern.

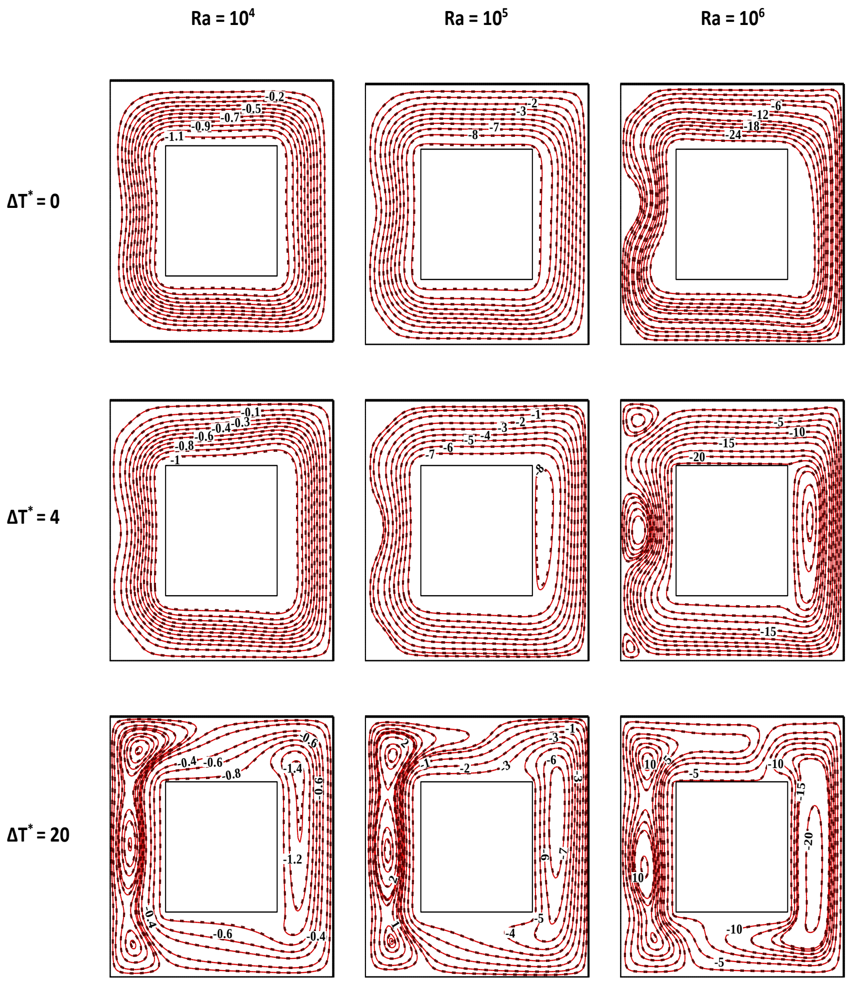

Figure 3. Streamlines for $SiO_2 - water$ (dotted line) and Co (solid line) with varying Ra and ΔT^* with $\varphi = 0.02, K^* = 2$, and $A^* = 0.25$.

Figure 4 illustrates the contour of isotherms for $10^4 \leq Ra \leq 10^6$ and $\Delta T^* = 0, 4$ and 20 with the fixed solid volume fraction ($\varphi = 0.02$) in which there does not exists any significant difference between the $SiO_2 - water$ nanofluid and Co ferrofluid thermal patterns. Furthermore it is found that for various Rayleigh number values ($10^4 \leq Ra \leq 10^6$) and temperature-difference ratio ($\Delta T^* = 0, 4$ and 20), dotted and solid lines tends to coincide with each other for the fixed solid volume fraction ($\varphi = 0.02$). Here, isotherms are uniformly distributed, and in the cases $\Delta T^* = 4$, $Ra = 10^5, 10^6$ and $\Delta T^* = 20$, $Ra = 10^4, 10^5$ and 10^6, the isotherms become denser inside the solid body. When $\Delta T^* = 4$ and $Ra = 10^4$ isotherms are confined together and for the cases $\Delta T^* = 0$, $Ra = 10^4, 10^5$ and 10^6, the isotherms disseminate throughout the enclosure.

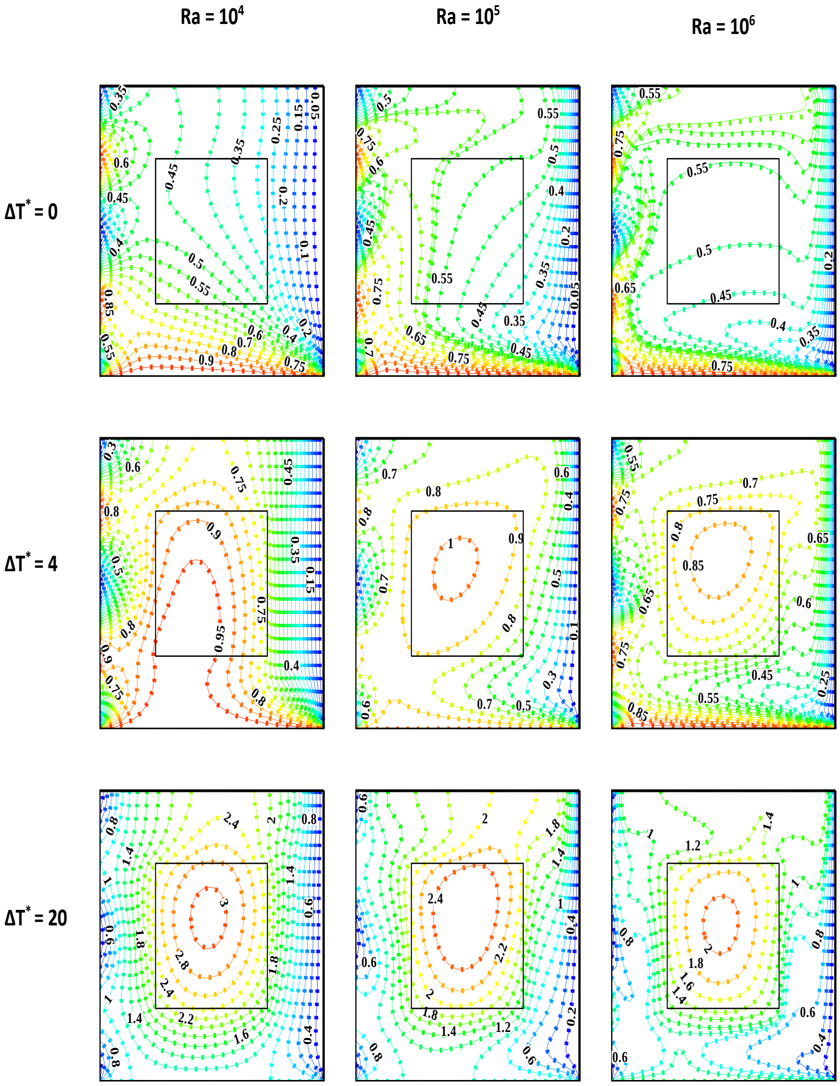

Figure 4. Isotherms for $SiO_2 - water$ (dotted line) and Co (solid line) with varying Ra and ΔT^* with $\varphi = 0.02, K^* = 2$, and $A^* = 0.25$.

Figure 5 illustrates the comparison between isotherms of $SiO_2 - water$ nanofluid and Co ferrofluid for $\varphi = 0.02, 0.1$ and 0.2 and $\Delta T^* = 0, 4$ and 20 with the fixed Rayleigh number $Ra = 10^5$. For the case $\Delta T^* = 0$, $\varphi = 0.02$ the streamlines contracts and confined towards the walls of square enclosure whereas in the cases $\Delta T^* = 0$, $\varphi = 0.1, 0.2$ and $\Delta T^* = 4$, $\varphi = 0.1$ and 0.2, there exists a implications between the $SiO_2 - water$ nanofluid and Co ferrofluid. In case of $\Delta T^* = 4$, $\varphi = 0.02$, an eddy is formed adjacent to right cold wall with significant difference which indicates that when the temperature-difference ratio increases streamlines turn to face the solid body's left side. For the cases $\Delta T^* = 20$, $\varphi = 0.02, 0.1$ and 0.2 four eddies are formed, which shows that fluid flow increases as the size factor of solid particles increases.

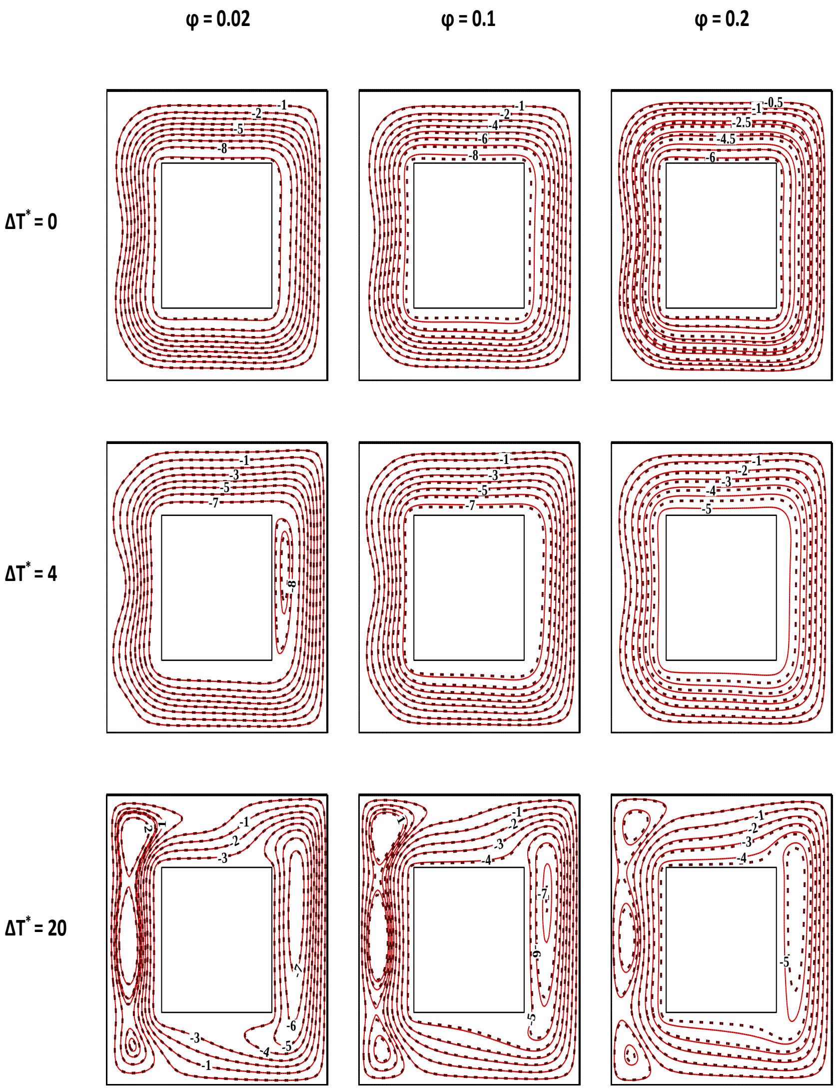

Figure 5. Streamlines for $SiO_2 - water$ (Dotted line) and Co (Solid line) with varying solid volume fraction (φ) and ΔT^* with $Ra = 10^5, K^* = 2, A^* = 0.25$.

Figure 6 depicts pattern of isotherms for $\varphi = 0.02$ and 0.1 and 0.2 and $\Delta T^* = 0, 4$ and 20 with the fixed Rayleigh number $Ra = 10^5$. For all ΔT^* and very low solid-volume fractions, there does not exist any significant difference in the isotherms, whereas for all ΔT^* and high-volume fractions, a small discrepancy between the isotherms is observed. In cases $\Delta T^* = 4,\ \varphi = 0.02$ and 0.1 and for $\Delta T^* = 20,\ \varphi = 0.02$, 0.1 and 0.2, the isotherms become more confined inside the solid body, and for the cases $\Delta T^* = 0,\ \varphi = 0.02, 0.1$ and 0.2 and $\Delta T^* = 4,\ \varphi = 0.2$, the isotherms get disseminated throughout the square enclosure. When the volume fraction increases, the Co ferrofluid flow is more effective then the nanofluid flow.

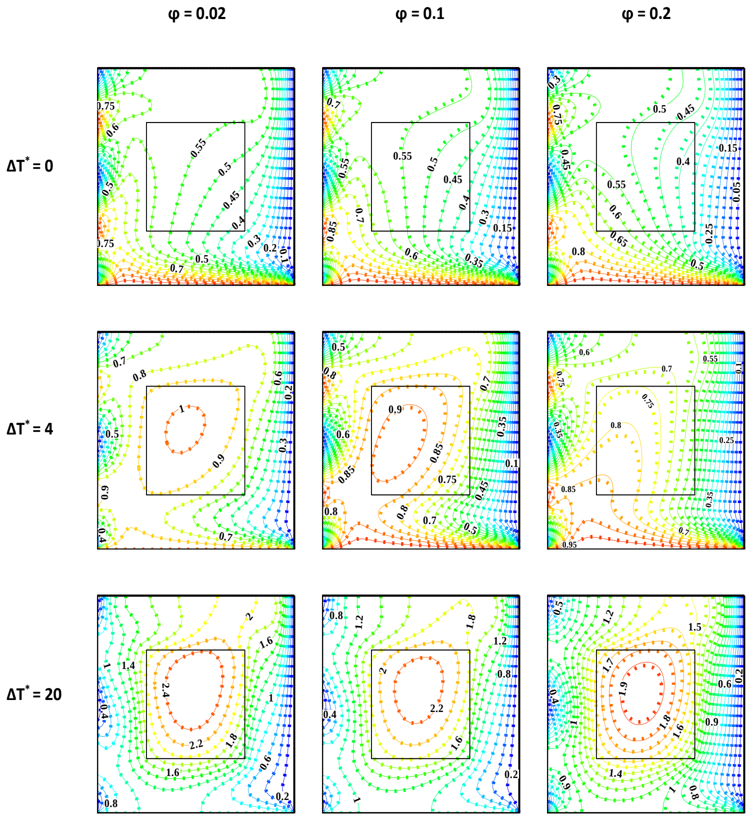

Figure 6. Isotherms for $SiO_2 - water$ (dotted line) and Co (solid line) with varying solid volume fractions (φ) and ΔT^* with $Ra = 10^5, K^* = 2$, and $A^* = 0.25$

Figure 7 depicts the correlation among the average Nusselt number with the temperature-difference ratio at a fixed solid volume fraction ($\varphi = 0.02$) and with varying Rayleigh number values along sinusoidal hot, constantly hot, and cold boundaries. Figure 7a shows that the temperature-difference ratio increases together with the average Nusselt number. Figure 7b shows that the average Nusselt number graph drops as the temperature-difference ratio rises. Figure 7c shows that when the temperature-difference ratio increases, the average Nusselt number decreases for the case of ($SiO_2 - water$) nanofluids, whereas for the case of Co ferrofluids, the average Nusselt number increases while the temperature-difference ratio declines. An identical heat-transfer rate was observed between $SiO_2 - water$ and Co ferrofluids.

Figure 8 shows the correlation between the temperature-difference ratio and the average Nusselt number for various solid particle sizes ($\varphi = 0.02, 0.1$ and 0.2) with the fixed Rayleigh number ($Ra = 10^5$), along with the sinusoidal, cold, and hot walls. Figure 8a shows that for the case of $SiO_2 - water$ nanofluids, the average Nusselt number graph drops as the temperature-difference ratio rises, whereas for the case of the Co ferrofluid flow the temperature-difference ratio decreases as the average Nusselt number rises. Figure 8b depicts that the average Nusselt number declines when the temperature-difference ratio increases, whereas a significant difference exists for $\varphi = 0.02$ and $\varphi = 0.1$. Figure 8c shows that as the average Nusselt number falls, the temperature-difference ratio increases for the $SiO_2 - water$ nanofluid, and for the Co ferrofluid, the average Nusselt number rises when the temperature-difference ratio rises.

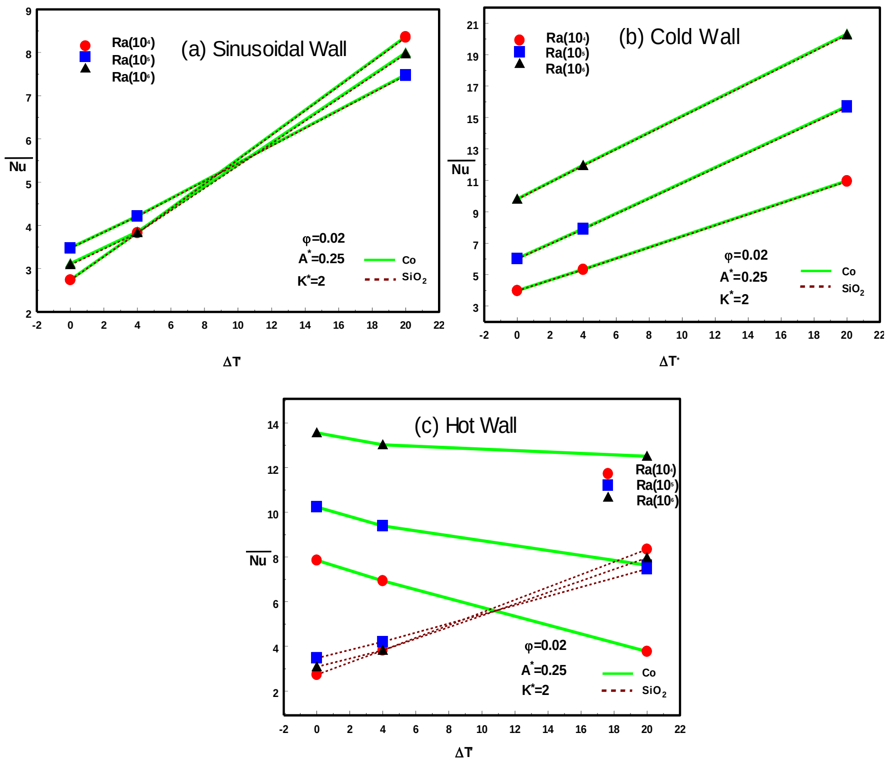

Figure 7. Variation of Nusselt number and Ra with $\varphi = 0.02$, $K^* = 2$, and $A^* = 0.25$.

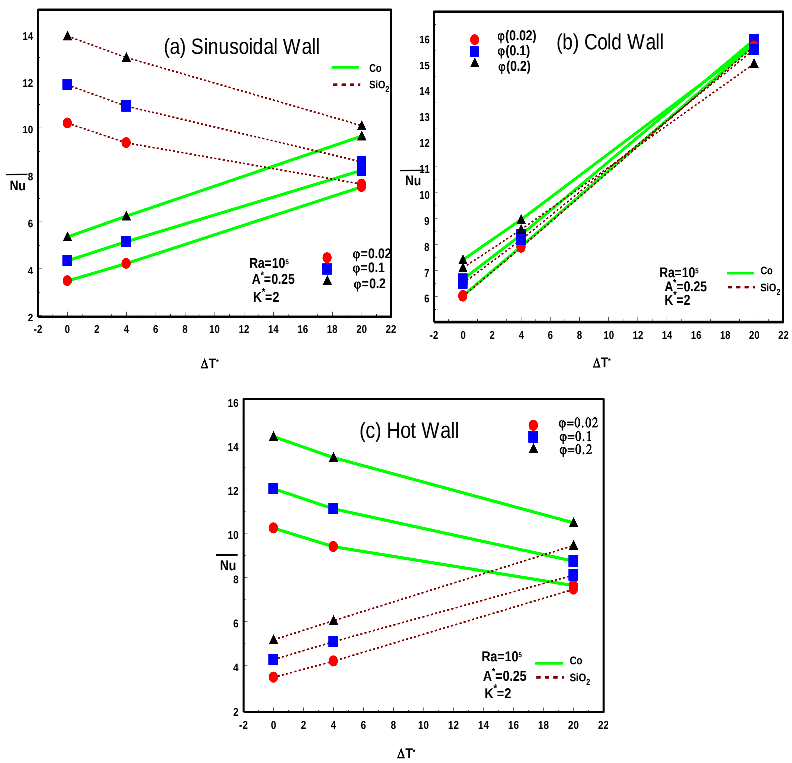

Figure 8. Variation of Nusselt number and solid volume fraction (φ) with $Ra = 10^5$, $K^* = 2$, and $A^* = 0.25$.

6. Conclusions

In the current research, a comparison between the $SiO_2 - water$ nanofluid and the Co ferrofluid is carried out by analyzing the impact of the different solid volume fraction and the Rayleigh number. In a square enclosure, the bottom wall is uniformly heated, the right side is cooled, the top wall is insulated, and the left wall is sinusoidally heated. As a result, the following were findings from the current study:

- No significant difference exists between the $SiO_2 - water$ nanofluid and the Co ferrofluid in the case of the increasing Rayleigh number, whereas there seems to be a noticeable difference between the $SiO_2 - water$ nanofluid and the Co ferrofluid in the case of boosting the solid volume fraction ;
- For both fluids, the strength of eddies grows as the temperature-difference ratio (ΔT^*) and the Rayleigh number (Ra) increase;
- For the case of the $SiO_2 - water$ nanofluid, the heat transmission rate decreases as tmperature-difference ratio (ΔT^*) inside the enclosure rises;
- While the temperature-difference ratio (ΔT^*) is decreased inside the enclosure, the heat transmission rate is increased for the Co ferrofluid.

Moreover, the work can be extended by including the magnetic field, and it is expected that this inclusion may enhance the thermal conductive property of $Co-$ of the ferrofluid. Additionally, this type of nanoparticle can be used for the situation where convection control is needed.

Author Contributions: Conceptualization, K.L. and U.P.; methodology, G.S.; software, U.P.; validation, U.P., N.A. and G.S.; formal analysis, N.A.; investigation, K.L.; resources, G.S.; data curation, G.S.; writing—original draft preparation, U.P. and K.L; writing—review and editing, N.A.; visualization, K.L.; supervision, K.L.; project administration, N.A.; funding acquisition, N.A. All authors have read and agreed to the published version of the manuscript.

Funding: Princess Nourah Bint Abdulrahman University Researchers Supporting Project number (PNURSP2022R59), Princess Nourah Bint Abdulrahman University, Riyadh, Saudi Arabia.

Institutional Review Board Statement: Not applicable.

Informed Consent Statement: Not applicable.

Data Availability Statement: Not applicable.

Acknowledgments: Princess Nourah Bint Abdulrahman University Researchers Supporting Project number (PNURSP2022R59), Princess Nourah Bint Abdulrahman University, Riyadh, Saudi Arabia.

Conflicts of Interest: The authors declare no conflict of interest.

Nomenclature

Alphabets

A	Amplitude
A^*	Area ratio
C_p	Specific heat $(\text{JKg}^{-1}\text{K}^{-1})$
U', V'	Non-dimensional velocity components
g	Acceleration due to gravity (ms^{-2})
X', Y'	Non-dimensional co-ordinates
k	Thermal conductivity $(\text{Wm}^{-1}\text{K}^{-1})$
K^*	Thermal conductivity ratio
L	Length of the enclosure (m)
$\overline{Nu}$	Average Nusselt number
P'	Non-dimensional pressure
Ra	Rayleigh number
Pr	Prandtl number
$\dot{q}$	Heat-generation per unit volume

T'	Temperature (K)
ΔT^*	Temperature-difference ratio
W	Width of the solid body
Greek symbols	
α	Thermal diffusivity (m^2s^{-1})
β	Thermal expansion coefficient (K^{-1})
θ'	Non-dimensional temperature
μ	Dynamic viscosity (Nsm^{-2})
ν	Kinematic viscosity (ms^{-2})
ρ	Density (kgm^{-3})
φ	Solid volume fraction
σ	Electrical conductivity (A m/V)
Subscripts	
c	Cold wall
h	Hot wall
f	Fluid
nf	Nanofluid
p	Particle
s	Solid

References

1. Jahanshahi, M.; Hosseinizadeh, S.F.; Alipanah, M.; Dehghani, A.; Vakilinejad, G.R. Numerical simulation of free convection based on experimental measured conductivity in a square cavity using $water/SiO_2$ nanofluid. *Int. Commun. Heat Mass Transf.* **2010**, *37*, 687–694. [CrossRef]
2. Sheikhzadeh, G.A.; Arefmanesh, A.; Kheirkhah, M.H.; Abdollahi, R. Natural convection of $Cu - water$ nanofluid in a cavity with partially active side walls. *Eur. J. Mech. B/Fluids* **2011**, *30*, 166–176. [CrossRef]
3. Aminossadati, S.M.; Ghasemi, B. Natural convection of $water - CuO$ nanofluid in a cavity with two pairs of heat source sink. *Int. Commun. Heat Mass Transf.* **2011**, *38*, 672–678. [CrossRef]
4. Haddad, Z.; Oztop, H.F.; Abu-Nada, E.; Mataoui, A. A review on natural convective heat transfer of nanofluids. *Renew. Sustain. Energy Rev.* **2012**, *16*, 5363–5378. [CrossRef]
5. Basak, T.; Chamkha, A.J. Heatline analysis on natural convection for nanofluids confined within square cavities with various thermal boundary conditions. *Int. J. Heat Mass Transf.* **2012**, *55*, 5526–5543. [CrossRef]
6. Garoosi, F.; Rohani, B.; Rashidi, M.M. Two-phase mixture modeling of mixed convection of nanofluids in a square cavity with internal and external heating. *Powder Technol.* **2015**, *275*, 304–321. [CrossRef]
7. Hasan, M.N.; Samiuzzaman, K.; Haque, S.H.; Saha, S.; Md, Q.I. Mixed convection heat transfer inside a square cavity filled with $Cu - water$ nanofluid. *Procedia Eng.* **2015**, *105*, 438–445. [CrossRef]
8. Umadevi, P.; Nithyadevi, N. Convection in a sinusoidally heated square enclosure utilizing $Ag - water$ nanofluid with heat-generating solid body. *Int. J. Mech. Sci.* **2017**, *131–132*, 712–721. [CrossRef]
9. Guestal, M.; Kadja, M.; Hoang, M.T. Study of heat transfer by natural convection of nanofluids in a partially heated cylindrical enclosure. *Case Stud. Therm. Eng.* **2018**, *11*, 135–144. [CrossRef]
10. Bairi, A.; Laraqi, N.; Adeyeye, K. Thermal behavior of an active electronic dome contained in a tilted hemispherical enclosure and subjected to nanofluidic Cu-Water free convection. *Eur. Phys. J. Plus*. **2018**, *133*, 93. [CrossRef]
11. Mashayekhi, R.; Gholami, M.; Khodabandeh, E.; Akbari, O.A.; Toghraie, D.; Bahiraei, M. CFD analysis of thermal and hydrodynamic characteristics of hybrid nanofluid in a new designed sinusoidal double-layered microchannel heat sink . *J. Therm. Anal. Calorim.* **2018**, 134, 2305–2315. [CrossRef]
12. Arasteh, H.; Mashayekhi, R.; Goodarzi, M.; Motaharpour, S.H.; Dahari, M.; Toghraie, D. Heat and fluid flow analysis of metal foam embedded in a double-layered sinusoidal heat sink under local thermal non-equilibrium condition using nanofluid. *J. Therm. Anal. Calorim.* **2019**, *138*, 1461–1476. [CrossRef]
13. Al-Srayyih, B.M.; Gao, S.; Hussain, S.H. Effects of linearly heated left wall on natural convection within a superposed cavity filled with composite nanofluid porous layers. *Adv. Powder Technol.* **2019**, *30*, 55–72. [CrossRef]
14. Latifa, M.; Al-Balushi; Uddin, M.J.; Rahman, M.M. Natural convective heat transfer in a square enclosure utilizing magnetic nanoparticles. *Propuls. Power Res.* **2019**, *8*, 194–209. [CrossRef]
15. Fu, Z.J.; Tang, Z.C.; Zhao, H.T.; Li, P.W.; Rabczuk, T. Numerical solutions of the coupled unsteady nonlinear convection-diffusion equations based on generalized finite difference method. *Eur. Phys. J. Plus* **2019**, *134*, 272. [CrossRef]
16. Massoudi, M.D.; Hamida, M.B.B. MHD Natural convection and thermal radiation of diamond-water nanofluid around rotating elliptical baffle inside inclined trapezoidal cavity. *Eur. Phys. J. Plus.* **2020**, *135*, 902. [CrossRef]
17. Lee, M.; Kim, Y.J. Effect of non-uniform magnetic fields on the characteristics of ferrofluid flow in a square enclosure. *J. Magn. Magn. Mater.* **2020**, *506*, 166697. [CrossRef]

18. Mourad, A.; Aissa, A.; Oudina, F.M.; Kouz, W.A.; Sahnoun, M. Natural convection of nanoliquid from elliptic cylinder in wavy enclosure under the effect of uniform magnetic field: Numerical investigation. *Eur. Phys. J. Plus*. **2021**, *136*, 429. [CrossRef]
19. Chandanam, V.; Lakshmi, C.V.; Venkatadri, K.; Beg, O.A.; Prasad, V.R. Numerical simulation of thermal management during natural convection in a porous triangular cavity containing air and hot obstacles. *Eur. Phys. J. Plus* **2021**, *136*, 885. [CrossRef]
20. Javed, T.; Siddiqui, M.A. Effect of MHD on heat transfer through ferrofluid inside a square cavity containing obstacle/heat source. *Int. J. Therm. Sci.* **2011**, *50*, 1748–1756. [CrossRef]
21. Pal, G.C.; Nammi, G.; Pati, S.; Baranyi, P.R.R.L. Natural convection in an enclosure with a pair of cylinders under magnetic field. *Case Stud. Therm. Eng.* **2021**, *30*, 101763. [CrossRef]
22. Ho, C.J.; Huang, C.Y.; Lai, C.M. Heat Transfer by Natural Convection in a Square Enclosure Containing PCM Suspensions. *Energies* **2021**, *14*, 2857. [CrossRef]
23. Govindarao, N.; Deka, D.K.; Pati, S.; Baranyi, L. Natural convection heat transfer within a square porous enclosure with four heated cylinders. *Case Stud. Therm. Eng.* **2021**, *30*, 101733. [CrossRef]
24. Mashkour, M.A.; Hadi, J.M.; Jary, A.M.; Habeeb, L.J. Review on natural convection heat transfer in an enclosures and cavities. *J. Mech. Eng. Res. Dev.* **2021**, *44*, 372–378.
25. Ghoben, Z.K.; Hussein, A.K. Natural convection inside a 3D regular shape enclosures—A brief review. *Int. J. Heat Technol.* **2022**, *40*, 232–246. [CrossRef]
26. House, J.M.; Beckermann, C.; Smith, T.F. Effect of a centered conducting body on natural convection heat transfer in an enclosure. *Numer. Heat Transf. Part A Appl.* **1990**, *18*, 213–225. [CrossRef]
27. Brinkman, H.C. The Viscosity of concentrated suspensions and solution. *J. Chem. Phys.* **1952**, *20*, 571–581. [CrossRef]
28. Maxwell, J. *A Treatise on Electricity and Magnetism*, 2nd ed.; Oxford University Press: Cambridge, UK, 1904.
29. Patankar, S.V. *Numerical Heat Transfer and Fluid Flow*; Hemisphere McGraw-Hill: Washington, DC, USA, 1980.
30. Cheikh, N.B.; Chamkha, A.J.; Beya, B.B.; Lili, T. Natural convection of water-based nanofluids in a square enclosure with non-uniform heating of bottom wall. *J. Mod. Phys.* **2013**, *4*, 147–159. [CrossRef]